AD-A274 594

②

FINAL TECHNICAL REPORT

NONLINEAR HYSTERESIS IN AN ENDOCHRONIC SOLID

INSTITUTE OF GEOPHYSICS AND PLANETARY PHYSICS
SCRIPPS INSTITUTION OF OCEANOGRAPHY, A-025
UNIVERSITY OF CALIFORNIA SAN DIEGO
LA JOLLA, CA 92093-0225

DTIC
ELECTE
S
JAN 1 1 1994
C
D

CONTRACT NUMBER :   F19628-88-K-0039

CONTRACT PERIOD: NOVEMBER 3, 1991, TO NOVEMBER 3, 1993

PRINCIPAL INVESTIGATORS: JEAN-BERNARD MINSTER   (619) 534-5650

94-01140

94 1 10 11 2

REPORT DOCUMENTATION PAGE

1 AGENCY USE ONLY (Leave blank)	2. REPORT DATE 1/4/94	3. REPORT TYPE AND DATES COVERED 11/3/91– Final Technical Report 11/3/93

4. TITLE AND SUBTITLE	5. FUNDING NUMBERS
NONLINEAR HYSTERESIS IN AN ENDOCHRONIC SOLID	PE 62714 E PR 8A10 TA DA WVAR Contract # F19628-88-K-0039

6. AUTHOR(S)

JEAN-BERNARD MINSTER

7. PERFORMING ORGANIZATION NAME(S) AND ADDRESS(ES) The Regents of the University of California Scripps Institution of Oceanography Institute of Geophysics and Planetary Physics 0225 9500 Gilman Drive, La Jolla, CA 92093	8. PERFORMING ORGANIZATION REPORT NUMBER F19628-88-K-0039

9. SPONSORING/MONITORING AGENCY NAME(S) AND ADDRESS(ES) Defense Advanced Research Project Agency Nuclear Monitoring Research Office Department of the Air Force Phillips Laboratory, Hanscom AFB, MA 01731-5000 Contract Manager: James F. Lewkowicz, LWH	10. SPONSORING/MONITORING AGENCY REPORT NUMBER

11. SUPPLEMENTARY NOTES

12a. DISTRIBUTION/AVAILABILITY STATEMENT Approved for public release, distribution unlimited	12b. DISTRIBUTION CODE

13. ABSTRACT (Maximum 200 words)

Propagation of seismic waves in the nearfield where rock rheology is demonstrably nonlinear raises unique difficulties. Nonlinearity arises primarily in two forms at intermediate to large strains: (1) nonlinear elasticity, and (2) amplitude-dependent attenuation. The proper representation of nonlinear constitutive equations for rocks in this regime is a potentially important ingredient of quantitative source models. We have shown previously that nonlinear one-dimensional wave propagation can result in spectral distortions at all wavelengths. This effect is strongly pulse-shape dependent, and therefore calls for a 3-D capability. More recently, we found that our approximate description of the phenomenology in the nonlinear regime was inadequate and unable to simulate new laboratory observations. We describe an intrinsically nonlinear rheological model, based on the endochronic framework of K. Valanis, which replicates the main features of observed hysteresis loops in the strain regime of interest and is easily reduced to differential form. The resulting differential equations can be readily solved numerically. Thus, this model is suitable for finite difference and finite element stress wave codes. Ultimately, a complete description of the rheology in terms of a thermodynamically valid constitutive equation is really what should be used in numerical simulations, if it can be developed and validated experimentally.

This research was also supported by DOE, under LLNL Contract No. B157346, and LLNL UC Master Task Agreement, Task #4.

14. SUBJECT TERMS Rock mechanics, nonlinear rheology, source medium properties	15. NUMBER OF PAGES 15
	16. PRICE CODE

17. SECURITY CLASSIFICATION OF REPORT unclassified	18. SECURITY CLASSIFICATION OF THIS PAGE unclassified	19. SECURITY CLASSIFICATION OF ABSTRACT unclassified	20. LIMITATION OF ABSTRACT

Summary

Propagation of seismic waves in the nearfield where rock rheology is demonstrably nonlinear raises unique difficulties. .Nonlinearity arises primarily in two forms at intermediate to large strains: (1) nonlinear elasticity, and (2) amplitude-dependent attenuation, which is a well documented behavior at intermediate strains and low confining pressure. The proper representation of nonlinear constitutive equations for rocks in this regime is a potentially important ingredient of quantitative source models.

We have shown in previous work that nonlinear one-dimensional wave propagation can result in spectral distortions at all wavelengths, but that this effect is strongly pulse-shape dependent, and therefore call for a 3-D capability [*Minster et al.*, 1991]. These results have been given in previous reports. More recently, we have found that our use of an approximate description of the phenomenological behavior of rocks in the nonlinear regime was flawed insofar as it is not able to simulate new high-quality laboratory observations of hysteresis loops in both Sierra White granite and Berea sandstone [*Day et al.*, 1992]. Ultimately, a complete description of the rheology in terms of a thermodynamically valid constitutive equation is really what should be used in numerical simulations, if it can be developed and validated experimentally.

In this report, we described an approach based on an intirinsically nonlinear phenomenological model, based on the endochronic framework of K. Valanis [e.g. *Valanis and Read*, 1979]. This model shows considerable success in replicating the main features of observed hysteresis loops in rock in the strain regime of interest. Equally important, the model is readily reduced to differential form, and we have demonstrated that the resulting differential equations can be readily solved numerically. Thus, this model is suitable for incorporation into finite difference and finite element stress wave codes. Note that numerical simplicity, efficiency, and stability are essential characteristics of a model which is to be of practical utility.

Accesion For		
NTIS CRA&I		☑
DTIC TAB		☐
Unannounced		☐
Justification		
By		
Distribution /		
Availability Codes		
Dist	Avail and / or Special	
A-1		

ii

Nonlinear Hysteresis in an Endochronic Solid

Steven M. Day
San Diego State University, San Diego, CA

Jean-Bernard Minster, Michael Tryon, and Lois Yu
Scripps Institution of Oceanography, IGPP, La Jolla, CA 92093

1. OBJECTIVES

Propagation of seismic waves in the nearfield where rock rheology is demonstrably nonlinear raises unique difficulties. Nonlinearity arises primarily in two forms at intermediate to large strains: (1) nonlinear elasticity, and (2) amplitude-dependent attenuation, which is a well documented behavior at intermediate strains and low confining pressure. The proper representation of nonlinear constitutive equations for rocks in this regime is a potentially important ingredient of quantitative source models.

Stress wave propagation and attenuation, in rocks and soils, show evidence of significant nonlinearity at strain amplitudes as low as 10^{-6}, leading in particular to an amplitude dependence of the apparent Q, most likely associated with friction along microcracks and joints [e.g. *Boitnott*, 1992]. Recent quasistatic laboratory testing of rock at low strain has permitted detailed high-quality observations of cusped hysteresis loops in this regime. These issues have been recently reviewed by *Minster et al.* [1991] and summarized by *Martin and Minster* [1992]. Nonlinear wave propagation in geological materials has also been observed and modeled in a different context by *Bonner and Wannamaker* [1991], and by *Johnson et al.* [1991]. Our objective is to identify and validate a rheological model (constitutive equation) for rocks, valid at moderate strains, that explains satisfactorily these various observations, and is appropriate for incorporation in numerical source and wave propagation codes, and apply the rheological model to improve our understanding of seismic source physics.

We have shown in previous work that nonlinear one-dimensional wave propagation can result in spectral distortions at all wavelengths, but that this effect is strongly pulse-shape dependent, and therefore call for a 3-D capability [*Minster et al.*, 1991]. More recently, we have found that our use of an approximate description of the phenomenological behavior of rocks in the nonlinear regime is flawed insofar as it is not able to simulate new high-quality laboratory observations of hysteresis loops in both Sierra White granite and Berea sandstone [*Day et al.*, 1992]. Ultimately, a complete description of the rheology in terms of a thermodynamically valid constitutive equation is really what should be used in numerical simulations, if it can be developed and validated experimentally.

2. NONLINEAR WAVE PROPAGATION AND ATTENUATION

Our earlier numerical modeling of nonlinear attenuation in the intermediate strain regime used viscoelastic theory as its point of departure [*Minster and Day*, 1986; *Minster et al.* 1991]. We review that approach here, in order to highlight its analogies as well as its contrasts with the new approach proposed in Section 4. A further reason for reviewing the numerical approach to viscoelasticity is that, to be acceptable, a model for the nonlinear intermediate strain regime should be well behaved in the low strain limit. Thus, it will be desirable to develop a numerical wave propagation treatment which reduces to linear viscoelasticity in the small amplitude limit.

2.1 *Broad-band approximation of amplitude-dependent attenuating rheology*

Based on a suite of one-dimensional simulations of nonlinear wave propagation problems *Minster et al.* [1991] concluded that a simple model in which Q^{-1} is simply

assumed to be proportional to strain amplitude can explain the shape distortion of Lorentz peaks observed in the laboratory at moderate strains, and the apparent superposability of simple pulses even in the nonlinear regime. They also concluded that, in contrast to linear Q models for which the spectrum of the "Q operator" tends to unity at low frequencies, a nonlinear rheology may lead to significant spectral distortions *at all frequencies*, and energy losses can be substantial even at wavelengths long compared to the propagation distance. Thus, even though nonlinear rheology is only relevant within a limited distance from a seismic source, this raises the possibility that the far field source spectrum can be affected to some degree at all frequencies, including those pertinent to regional phases and teleseismic body waves.

Those results were based on an attenuation model described by

$$Q^{-1} = Q_a^{-1} + \gamma \varepsilon \quad , \tag{2.1}$$

where ε is the strain amplitude, γ is a material constant, and Q_a^{-1} represents a linear anelastic term controlled by mechanisms that mask the nonlinear ones at low strain. This form of amplitude-dependence describes well the bulk of laboratory evidence accumulated to date. Nonlinear wave propagation simulations were conducted in two steps. First, we used the Padé approximant method of *Day and Minster* [1984] to convert the stress-strain relation of a linear, anelastic solid, with frequency-independent Q, into differential form. An absorption band, with Q nearly constant at Q_0, and with minimum and maximum relaxation times τ_1 and τ_2, respectively, yields the following relation between stress history, $\sigma(t)$ and strain history, $\varepsilon(t)$

$$\sigma(t) = \int_0^t M_u \left[1 - \frac{2}{\pi Q_0} \int_{\tau_1}^{\tau_2} \left(1 - e^{-(t-t')/\tau} \right) \frac{d\tau}{\tau} \right] d\varepsilon(t') \quad , \tag{2.2}$$

where M_u is the unrelaxed modulus. We showed that (2.2) can be approximated by

$$\sigma(t) = M_u \left[\varepsilon(t) - \sum_{i=1}^n \zeta_i(t) \right] \quad , \tag{2.3}$$

where the ζ_i's are relaxation terms governed by the n linear equations

$$\frac{d\zeta_i}{dt} + \nu_i \zeta_i = \frac{\tau_1^{-1} - \tau_2^{-1}}{\pi} w_i \, Q_0^{-1} \, \varepsilon(t) \quad , \tag{2.4}$$

The constants ν_i and w_i which depend on the order of approximation, n, are given by *Day and Minster* [1984], who also show that the operator defined by (2.3) and (2.4) converges to the exact result (2.2) as n increases. The second step is to generalize (2.4) by introducing a linear dependence of Q_0 on strain amplitude according to (2.1):

$$\frac{d\zeta_i}{dt} + \nu_i \zeta_i = \frac{\tau_1^{-1} - \tau_2^{-1}}{\pi} w_i \left(Q_a^{-1} + \gamma |\varepsilon(t)| \right) \varepsilon(t) \quad . \tag{2.5}$$

Then, (2.3) and (2.5) constitute the stress-strain equations for our one-dimensional finite difference simulations.

All differential operators generated by this procedure can be guaranteed to be causal, stable, and dissipative. However, that the method performs rather poorly when the absorption band is much broader than the calculational pass band, that is, the interval between the maximum and minimum frequencies resolvable by the numerical method. For example, the finite difference method is limited to the frequency band from $1/n\delta t$ to

roughly $1/m\delta t$, where δt is the time step, n is the total number of time steps computed, and m is the number of time steps associated with the minimum resolvable wavelength; m is typically of the order of 20, and n may be up to several thousand for large two-dimensional calculations. We have devised a simple extension of the method which renders it suitable for broad absorption bands, without compromising its analytical and numerical simplicity. Using the Laplace transform in s-multiplied form, we reduce the stress-strain relation to its operational form:

$$\bar{\sigma}(s) = \bar{M}(s)\, \bar{\varepsilon}(s) \tag{2.6}$$

Note that the operational modulus $\bar{M}$ has the same dimensions as the step response M. The unrelaxed modulus M_u, the relaxed modulus M_R, the modulus defect, δM, and the normalized relaxation function ϕ, are given by

$$M_u = M(0) = \bar{M}(\infty) \tag{2.7}$$

$$M_R = M(\infty) = \bar{M}(0) \tag{2.8}$$

$$\delta M = M_u - M_R \tag{2.9}$$

$$M(t) = M_R + \delta M\, \phi(t) \tag{2.10}$$

We represent the relaxation function in terms of a relaxation spectrum Φ,

$$\phi(t) = \int_{-\infty}^{\infty} \Phi(\ln \tau)\, exp(-t/\tau)\, d(\ln \tau) \tag{2.11}$$

resulting in the following integral expression for the operational modulus:

$$\bar{M}(s) = M_u - \delta M \int_0^{\infty} \frac{\hat{\Phi}(p)\, dp}{s + p} \tag{2.12}$$

where $\hat{\Phi}(p) = \Phi(\ln \tau^{-1})$. We may now partition of the p integral into 3 regimes, separated by low-frequency cutoff p_{min} and high-frequency cutoff p_{max})

$$\bar{M}(s) = M_u - \delta M\, (I_1 + I_2 + I_3) \tag{2.13}$$

$$I_1 = \int_0^{p_{min}} \frac{\hat{\Phi}(p)\, dp}{s + p} \quad I_2 = \int_{p_{min}}^{p_{max}} \frac{\hat{\Phi}(p)\, dp}{s + p} \quad I_3 = \int_{p_{max}}^{\infty} \frac{\hat{\Phi}(p)\, dp}{s + p} \tag{2.14,15,16}$$

The interval $(p_{min},\ p_{max})$ is prescribed to coincide with the calculational pass band. The middle partition, I_2, is replaced with an nth order Padé approximant, as before, but with the support interval of interval of Φ, $(\tau_2^{-1},\ \tau_1^{-1})$, replaced by the interval $(p_{min},\ p_{max})$ Then I_1 and I_3 are approximated by Taylor series about ∞ and 0, respectively. Laplace inversion leads to a representation of total stress as a sum of $n+2$ internal variables, each of which satisfies a first order differential equation. This permits us to model broad absorption bands efficiently and with much better accuracy than before.

3. LABORATORY OBSERVATIONS OF HYSTERESIS LOOPS

In order to validate the nonlinear models described above, we have conducted simulations of hysteresis loops measured at several strain amplitudes in uniaxial tests on

Sierra White granite and Berea sandstone. These data have been collected by New England Research Inc., and have been kindly made available to us by Drs. R. Martin, R. Haupt, and G. Boitnott. As reported by *Day et al.* [1992], these simulations brought to light a serious shortcoming of our approach, namely that it does not produce the correct loop shapes when the strain amplitude is increased into the nonlinear regime. Various modifications of our general approach-all resulted in failure, pointing to the need for a completely different treatment of the rheology, dealing *intrinsically* with the nonlinearity.

Laboratory stress-strain curves under cyclic loading characteristically exhibit the following features which a successful model must emulate:

- Hysteresis occurs, implying energy loss, and the effective Q characterizing this dissipation is strain-amplitude dependent.
- The hysteresis loops are cusped at reversal points, rather than elliptical (as would typify linear anelastic behavior).
- No yield surface is evident in the loading curves, at least for strains up to about 10^{-4}.
- Upon reversal of strain path, the tangent modulus is roughly equal to the instantaneous elastic modulus.

Typical raw laboratory data in the form of stress and strain histories are often rather noisy, and require filtering. Simple low-pass filtering smoothes the cusps, thereby masking the onset of nonlinear behavior, and affecting the measurement of moduli at and near the cusps. We have therefore developed a technique to filter separately the loading and unloading portions of the loops. It relies on the construction of a longer time series out of a half-loop—that is a portion of stress-strain history between two reversals, in which both stress and strain are monotonic. This is done by extending it in both directions with versions of itself, rotated by $\pm\pi$ about its end points. The extended time series is then de-meaned, de-trended, and low-pass filtered using a phaseless filter to avoid introduction of a phase shift. The filtered version is truncated to the original length after restoring trend and mean, and the stress-strain path reconstructed by concatenation of filtered segments. The rotation by $\pm\pi$ of the extensions has the advantage of preserving the continuity of the time series and its derivative, thereby limiting undesirable end effects. It is important to avoid introducing cusps into hysteresis loops when they are not present, and to avoid smoothing through a cusp or changing its angle, when one is present. Too strong a filter will change the slope near the end points, and therefore introduce a fictitious cusp. Misapplication of the technique is detectable because this will create overlaps or gaps between successive segments. The technique gives very satisfactory results for noise levels as large as 10 percent as we have been able to verify using synthetic loops contaminated with additive noise. This approach facilitates considerably the estimation of the tangent modulus, particularly near the loop ends where noise contamination is most worrisome.

Several of the features described above are evident in Figures 1 and 2, which show selected sequences of hysteresis loops in Berea Sandstone and in Sierra White, respectively, under uniaxial stress. In both instances, the strain and stress time histories are shown in the top frame, followed by the corresponding stress-strain paths (hysteresis loops) on an expanded scale, after removal of the mean slope, in order to emphasise the key nonlinear characteristics; the bottom frame illustrates the dependence of the tangent modulus on strain. In the filtered data, the cusped nature of the reversal points is evident. Also evident is the near-equality of the initial loading and unloading slopes. The results illustrate clearly the non-elliptical (nonlinear) character of the hysteresis loops at such moderate strain levels, and also bring out clearly the strain hardening which causes the loops to show upward concavity.
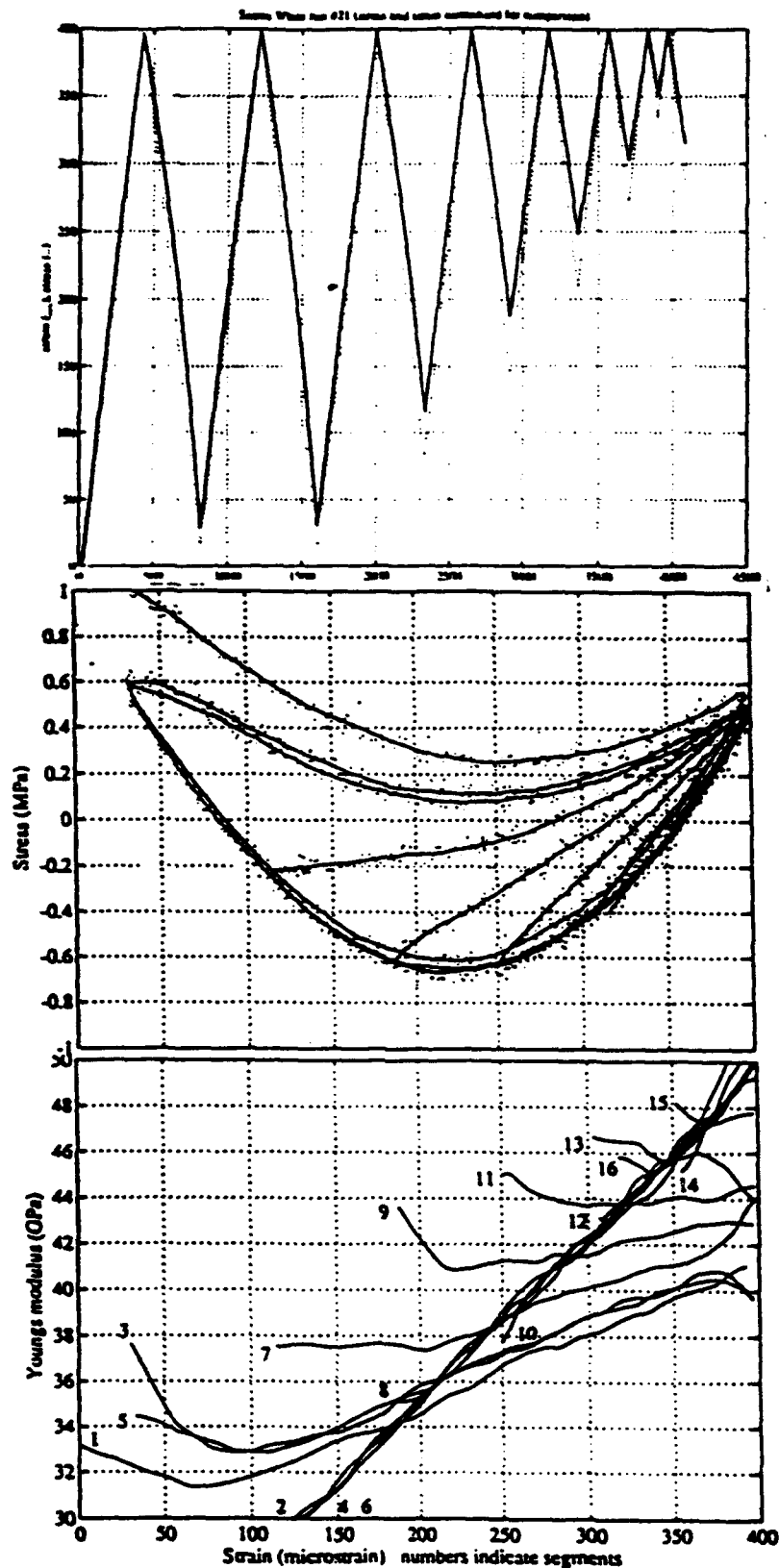
4

Figure 1: (a) Strain (solid line) and stress (dotted line) time histories for a uniaxial stress test on Sierra White granite. (b) corresponding stress and strain path, after smoothing; raw data are indicated by the dots, and the mean slope(modulus) of the hysteresis loops has been removed to emphasize the nonlinear characteristics. (c) Young's modulus dependence on strain for this test. Numbers indicate the various segments in the loading history, separated by path reversals.
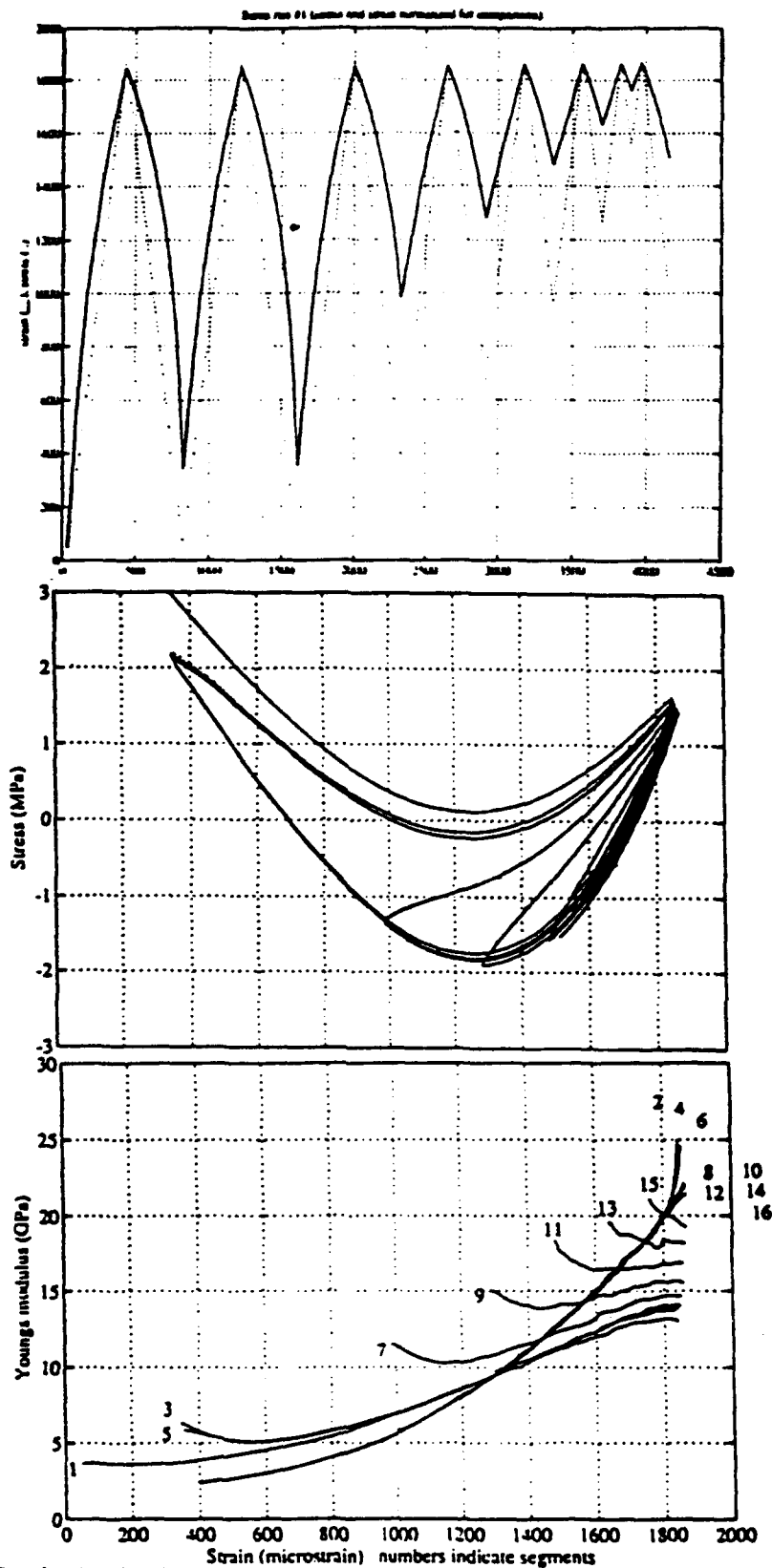
Figure 2: (a) Strain (solid line) and stress (dotted line) time histories for a uniaxial stress test on Berea Sandstone. (b) corresponding stress and strain path, after smoothing; raw data are indicated by the dots, and the mean slope(modulus) of the hysteresis loops has been removed to emphasize the nonlinear characteristics. (c) Young's modulus dependence on strain for this test. Numbers indicate the various segments in the loading history, separated by path reversals.

4. ENDOCHRONIC CONSTITUTIVE MODEL

4.1 Introduction

A successful rheological model should be capable of matching the features seen in Figures 1 and 2, which are often difficult to see in the raw data, but it should, as much as possible, avoid introducing a large number of additional model parameters for this purpose. The endochronic model described in this paper offers, we think, a very promising solution. In light of the observations outlined in the previous section, we have adopted an approach to modeling the moderate strain regime which departs sharply from viscoelastic models, yet retains much of the computational simplicity described in Section 2.

4.2 Background to the Endochronic Formulation

From the outset, we consider the class of constitutive models known as *simple materials*. With this restriction, the stress at a point depends only on the strain history at that point (not, for example, on strain gradients), i. e.,

$$\sigma(t) = F[e(t'),0 \leq t' \leq t]$$ (4.1)

where F is a functional relating the stress σ to the strain history $e(t)$. For example: if F is linear and time invariant, equation (1) reduces to a convolution, and we have the usual formulation of viscoelasticity:

$$\sigma(t) = M(t) * e(t)$$ (4.2)

This restriction combined with rate independence constitute sufficient conditions to ensure preservation of cube root scaling. To specialize 4.1 for a rate-independent simple material, we express the strain history in terms of the strain path length ξ. Then

$$\sigma(t) = F[e(\xi),\dot{\xi},0 \leq \xi(t') \leq \xi(t)]$$ (4.3)

The concept of rate-independence implies that there is no dependence of the rheology on the rate $\dot{\xi}$:

$$\sigma(t) = F[e(\xi), 0 \leq \xi(t') \leq \xi(t)]$$ (4.4)

where

$$d\xi = (de:g:de)^{1/2}$$ (4.5)

In other words, ξ is the strain path length, measured in terms of the metric g.

4.3 The Endochronic Material Model

Following *Valanis and Read* [1979], we consider the special case in which F is linear and shift-invariant in the *plastic* strain path length z

$$dz = (d\theta:g:d\theta)^{1/2}$$ (4.6)

where

$$d\theta = de - \frac{d\sigma}{2\mu}$$ (4.7)

is the plastic strain increment. The linear, shift-invariant assumption guarantees that we can write σ as a convolution over z; that is:

$$\sigma(t) = K(z) * \frac{d\theta}{dz}$$ (4.8)

If the kernel $K(z)$ is chosen to have an integrable singularity at $z = 0$, then all the features noted above are realized:

$$K(z) \propto z^{-\alpha}, 0 < \alpha < 1 \qquad (4.9)$$

It is the singular behavior of the kernel that insures that loading and unloading at reversal points occurs with stress-strain slope equal to the elastic modulus. Furthermore, as demonstrated below, we have been able to show that the singular kernel ensures power law dependence of Q^{-1} on strain amplitude, in accordance with experimental observations cited previously.

4.4 Amplitude-Dependence of Q in the Endochronic Model

The power law amplitude dependence of Q^{-1} is derived by noting that

$$\sigma \propto \int_0^z (z-z')^{-\alpha} \frac{d\theta(z')}{dz'} dz' \qquad (4.10)$$

Restricting treatment to uniaxial loading,

$$\left| \frac{d\theta}{dz} \right| = 1 \qquad (4.11)$$

so, in terms of the maximum plastic strain z_m,

$$\sigma \propto (z_m)^{1-\alpha} \qquad (4.12)$$

From the definition of Q^{-1} in terms of the area of the hysteresis loop, we obtain:

$$Q^{-1} \propto \frac{\sigma_m z_m}{\sigma_m^2}, \qquad (4.13)$$

and from 4.13 and 4.14, we obtain

$$Q^{-1} \propto (\sigma_m)^{\alpha/(1-\alpha)} \qquad (4.14)$$

Note that for $\alpha = 1/2$, we have an approximately linear dependence on strain amplitude, in agreement with a large body of laboratory observations. The endochronic model thus appears capable of emulating laboratory observations of hysteretic behavior, as well as amplitude dependence of attenuation at moderate strain amplitudes.

4.5 Computational approach

To be useful for numerical simulations, the convolution form 4.8 must be converted to a differential constitutive equation. Since the endochronic model has a formal structure similar to linear viscoelasticity, we can carry out this conversion in a manner analogous to that used in Section 2. That is, we first Laplace transform 4.8,

$$\overline{\sigma}(s) = s\overline{K}(s)\overline{\theta}(s) \qquad (4.15)$$

We approximate $\overline{K}(s)$ by a rational function $\overline{K}_n(s)$, where n is the order of the denominator. Then, we develop $\overline{K}_n(s)$ as a partial fraction expansion

$$\overline{K}_n(s) = \sum_{j=1}^{n} \frac{\lambda_j}{s + v_j}, \qquad (4.16)$$

where v_j and λ_j are the poles and residues, respectively, of $\overline{K}_n(s)$.

Transformation back to the z domain yields the following system of differential equations for σ:

8

$$\sigma(z) = \sum_{j=1}^{n} \zeta_j$$

$$\frac{d\zeta_j(z)}{dz} + v_j \zeta_j(z) = \lambda_j \frac{d\theta}{dz}$$

(4.17)

Equations 4.6, 4.7, and 4.17 form the set of constitutive equations which are solved numerically. A convenient numerical scheme for the solution of such a system is given by *Murakami and Read* [1989], and we have successfully implemented that scheme to compute the numerical results shown in the next section.

5. APPLICATION TO LABORATORY AND FIELD DATA

To validate the use of the endochronic model, we have conducted simulations of hysteresis loops measured at several strain amplitudes in uniaxial tests on Sierra White granite and Berea sandstone data collected by New England Research Inc.

Figure 3 shows a comparison of such simulations with three observed loops in Sierra White, at stress levels of 3, 6, and 12 bars, respectively. The numerical simulations (which are symmetrical in stress and strain histories) match well the overall character of the observations; this includes in particular the increase in attenuation with increasing strain.

Figure 4 shows a similar comparison for Berea sandstone, for which the attenuation levels are much higher, as illustrated by the loop areas. With respect to attenuation and loop shape, the comparison is quite favorable. The theoretical loops simulate the amplitude dependence of Q and the non-elliptical loop shapes, including cusps at the ends. The mean slope decreases somewhat more rapidly with increasing strain amplitude for the experimental loops than it does for the theoretical loops. Further improvement of the model fit to the Berea Sandstone data can be obtained by introducing variations into the shape of the kernel function.

We have also calculated Q^{-1} as a function of strain amplitude for both the Sierra White Granite and Berea Sandstone models. The Berea model produces Q^{-1} nearly proportional to strain amplitude over the full range shown. The present Sierra White model also exhibits a strong amplitude dependence of Q^{-1}, although it departs slightly from the expected linear dependence of Q^{-1} on strain amplitude. This is probably as a result of approximations introduced in our current expansion of the singular kernel function.

The singular kernel endochronic model reproduces several key nonlinear phenomena associated with rock hysteresis at moderate strain. The approach represents a substantial improvement over earlier attempts to simulate amplitude-dependent attenuation using variants of viscoelasticity. Although purely phenomenological, the endochronic approach has the decided advantage that it readily reduces to a set of relatively simple differential equations which are easily solved numerically. All numerical results reported here were obtained by solving this system of differential equations numerically. Exactly the same algorithm can be applied to compute stress-strain behavior in numerical wave propagation codes.
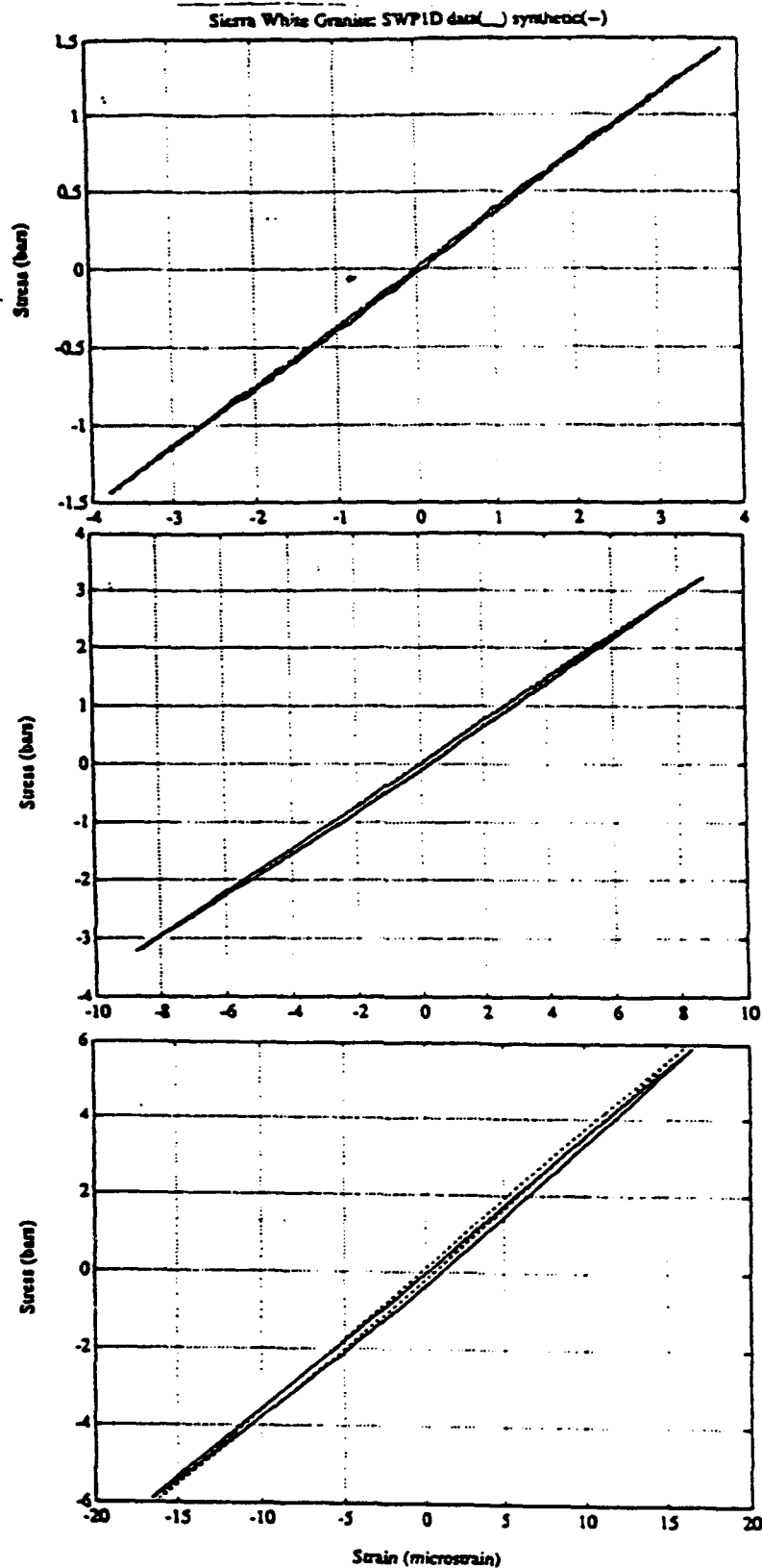
Figure 3: Comparison of endochronic simulations with three observed loops in Sierra White, at stress levels of 3, 6, and 12 bars, respectively. The numerical simulations (which are symmetrical in stress and strain histories) match well the overall character of the observations; this includes in particular the increase in attenuation with increasing strain. Additional simulations for larger stress amplitudes show that Q^{-1} continues to increase at large strain levels.
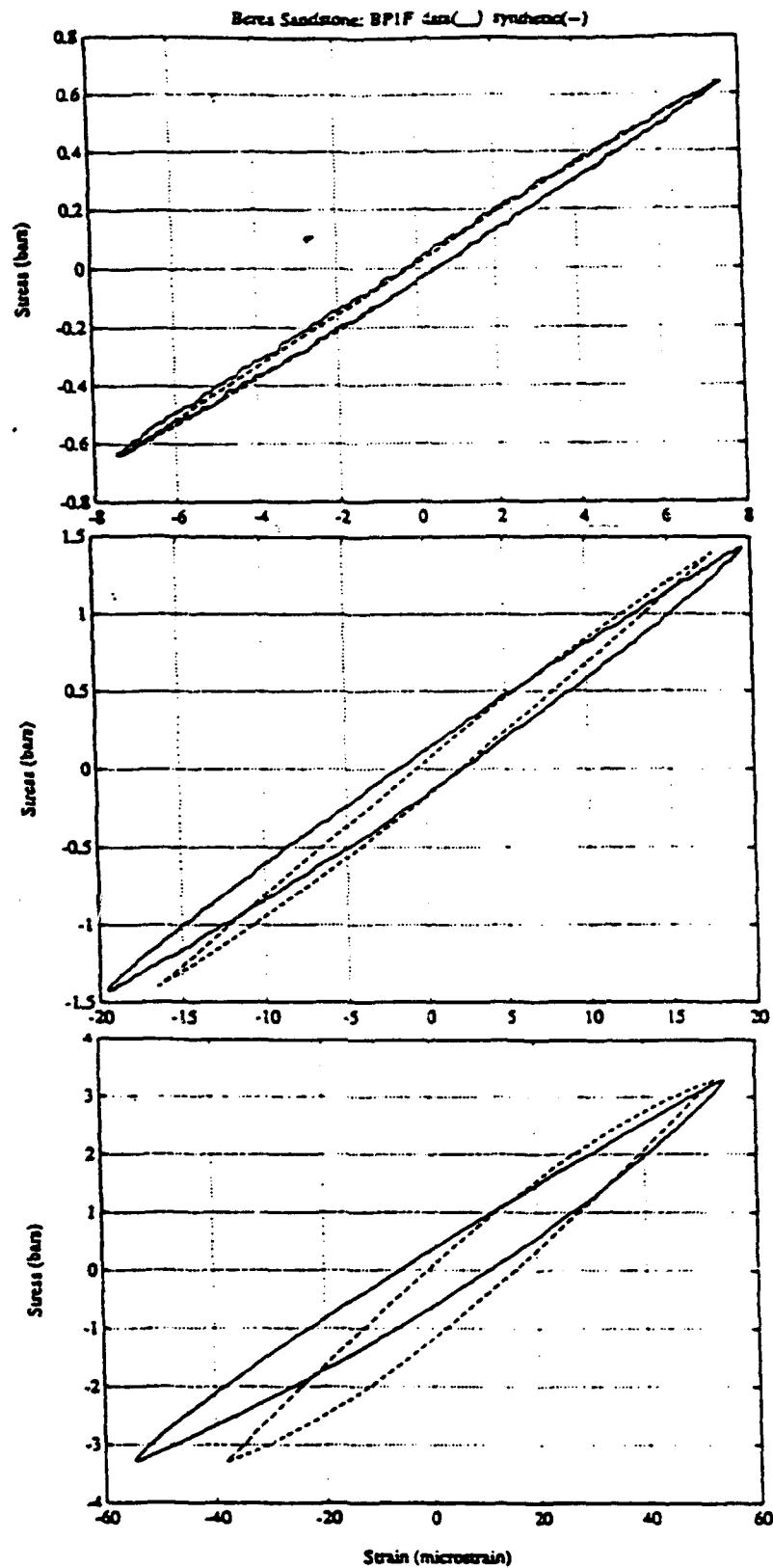
Figure 4: Similar comparison (see Figure 3) for Berea sandstone, for which the attenuation levels are much higher, as illustrated by the loop areas. Again, the comparison is quite favorable, including the amplitude dependence of Q, and the non elliptical loop shapes, with apparent cusps at the ends. It should be emphasized that, unlike many nonlinear models, the model used in these simulations depends only on a small number of parameters, once the kernel singularity is specified.

As stated before, a 1-D nonlinear numerical model is not easily generalized to 3-D. For stress wave propagation, there is much more to it than merely including geometrical spreading, because the rheology itself is amplitude-dependent. Applications of this class of algorithms to the interpretation of seismological data collected in the field require therefore development and validation of a full 3-D wave propagation capability. Intuition fails us, or is even misleading for nonlinear situations, so that it makes little sense to develop such a capability until the model has been fully verified on laboratory data in the 1-D situation. We will therefore defer such effort until later.

6. CONCLUSIONS

Existing theory for seismic wave propagation is almost exclusively linear, despite abundant experimental and observational evidence of nonlinear phenomena in earth materials for strain levels exceeding about 10^{-6}. Our long-term goal is to make a significant contribution to filling this gap in seismic theory. Our approach promises to provide a stable and efficient algorithm for numerical simulation of nonlinear wave propagation at intermediate strain levels, with computational requirements only modestly exceeding those of linear viscoelasticity. The method should enable numerical modeling to better account for near-source nonlinear phenomena, which in turn will improve our understanding of source physics for both earthquakes and buried explosions.

In particular, the importance of nonlinearity in the intermediate strain regime for detection, identification, and yield estimation of underground explosions remains a significant unresolved issue. Specific phenomena which should be considered include (1) the effects of nonlinear attenuation on surface reflections (e.g., "depth" phases such as pP and pS), both for sources sufficiently shallow, so that the nonlinear regime extends to the free surface, and for the case of strongly attenuating surface layers (soils); (2) effects of nonlinear attenuation on the efficiency of high frequency cavity decoupling; and (3) the effect of nonlinear attenuation on the spectral characteristics of regional seismic recordings from both shallow and overburied explosions. For example, *Taylor and Randall* [1989] have identified systematic spectral differences between regional seismograms from shallow explosions and overburied explosions at NTS. The spectra of regional phases play an important role in event identification in the context of a nonproliferation or even a CTBT treaty, and it is thus very important to establish the physical origin of such spectral differences. Our work is aimed ultimately at understanding such near-source effects.

This project is being undertaken in coordination with experimental work at New England Research Corporation (NER). Our modeling results will be used to help guide the design of subsequent NER experiments. Those model parameter which are found to be most critical in controlling the seismic signature of explosions should be identified and targeted for experimental study. Such collaboration has already been initiated, and all the data sets shown in this report have been made available as a result of it. Experiments conducted by NER to date have focused on uniaxial stress geometries. However, shear attenuation is most important in the Earth, so that future experiments in torsion are of particular importance, as well as experiments highlighting the effects of pore fluids and saturation, which are essential at low strains. We are particularly concerned with the ability of the endochronic model to accommodate such effects, in a phenomenological sense. In particular, we would prefer not to require a large number of additional parameters to achieve a reliable representation of the rheology in realistic circumstances. A carefully designed feedback between modeling and experimentation appears to be the appropriate strategy to achieve this goal.

7. REFERENCES

Boitnott, G. N., Nonlinear attenuation in the near-source region: characterization of hysteresis in the deformation of rock joints, *Proc. 14th DARPA/PL Seismic Res. Symposium*, 1992.

Bonner, B.P., and B.J. Wannamaker, Acoustic nonlinearities produced by a single macroscopic fracture in granite, *Rev. Prog. in Quant. Nondestructive Eval.* **10B**, 1861, 1991.

Day, S.M., J.B. Minster, and L. Yu, Numerical simulation of nonlinear attenuation using an endochronic formulation, *Proc. 14th DARPA/PL Seismic Res. Symposium*, 1992.

Day, S.M. and J.B. Minster, Numerical simulation of attenuated wavefields using a Padé approximant method, *Geophys. J. Roy. Astr. Soc.*, **78**, pp. 105-118, 1984.

Johnson P.A., A. Migliori and T.J. Shankland, Continuous wave phase detection for probing nonlinear elastic wave interactions in rocks, *J. Acoust. Soc. Amer.*, **89**, 598, 1991.

Martin R.J., and J.B. Minster, *Rheology of rocks at moderate strains with application to attenuation and source characterization*, NER conference report, Jan. 8, 1992.

Minster, J.B. and S.M. Day, Decay of wave fields near an explosive source due to high-strain, nonlinear attenuation, *J. Geophys. Res.*, **91**, pp. 2113-2122, 1986.

Minster, J.B., S.M. Day, S., and P.M. Shearer, The transition to the elastic regime in the vicinity of an underground explosion, *AGU monograph* XX (Proceedings of the 1989 DOE workshop on explosion seismic sources.), 229-238, 1991.

Murakami, H., and H. E. Read, A second-order numerical scheme for integrating the endochronic plasticity equations, *Computers and Structures, 31*, pp. 663, 1989.

Taylor, S.R. and G.E. Randall, The effects of spall on regional seismograms, *Geophys. Res. Lett.*, **16**, 211-214, 1989.

Valanis K.C., and H.E. Read, A new endochronic plasticity theory for soils, S-Cubed Rept. SSS-R-80-4294, 1979.